Aerosp. Sci. Technol. 5 (2001) 125–134

S1270-9638(00)01087-7/FLA

Multivariate interpolation for fluid-structure-interaction problems using radial basis functions

Armin Beckert [a,1], Holger Wendland [b]

[a] Institute of Aeroelasticity, German Aerospace Center (DLR), Bunsenstraße 10, 37073 Göttingen, Germany
[b] Institute for Applied Mathematics, University of Göttingen, 37073 Göttingen, Germany

Received 14 March 2000; revised and accepted 17 November 2000

Abstract

A multivariate interpolation scheme for coupling fluid (CFD) and structural models (FE) in three-dimensional space is presented using radial basis functions. For the purpose of numerical aeroelastic computations, a selection of applicable functions is chosen: a classical without compact support, and some recently presented smooth compactly supported radial basis functions. The scheme is applied to a typical static aeroelastic problem, the prediction of the equilibrium of an elastic wing model in transonic fluid flow. The resulting coupled field problem containing the fluid and the structural state equations is solved by applying a partitioned solution procedure. The structure is represented by finite elements and the related equations are solved using a commercial FE analysis code. The transonic fluid flow is described by the three-dimensional Euler equations, solved by an upwind scheme procedure.© 2001 Éditions scientifiques et médicales Elsevier SAS

aeroelasticity / fluid-structure-interaction / staggered algorithm / coupling scheme / multivariate interpolation / radial basis function

Zusammenfassung

Anwendung von Multivariaten Interpolationen basierend auf Radialen Basis Funktionen auf Strömung-Struktur-Kopplungsprobleme. Es wird eine konservative Methode zur Kopplung von räumlich dreidimensionalen, numerischen aerodynamischen (CFD) und elastomechanischen (FE) Modellen vorgestellt, die auf die Anwendung Multivariater Interpolationen mit Radialen Basisfunktionen beruht. Der Kopplungsalgorithmus erfüllt die Forderung nach Unabängigkeit von den Gleichungen, die das aerodynamische und elastomechanische Modell beschreiben und den entsprechenden Lösungsmethoden. Diese Eigenschaft erlaubt einen Austausch der aerodynamischen und elastomechanischen Modelle und Berechnungsverfahren.

Zur Vorhersage des statischen aeroelastischen Deformationsverhaltens eines Tragflügels wurde die Methode und eine Auswahl von Radialen Basisfunktionen – mit und ohne kompaktem Träger – in ein Verfahren zur Lösung der relevanten gekoppelten aeroelastischen Gleichungen integriert. Es wurden numerische Berechnungen durchgeführt, deren Ergebnisse hier mit entsprechenden experimentellen Daten verglichen werden. Der Vergleich zeigt eine gute Übereinstimmung der aus den numerischen Berechnungen und dem Experiment gewonnenen Ergebnisse.

Für den gewählten Testfall und bei Betrachtung der Ergebnisse, die durch die Aufbringung der gemessenen Druckverteilung erzielt wurden, wies die C^2 Funktion von Wendland die geringsten Abweichungen auf. Die Klasse der Funktionen mit Trägereigenschaft zeigte hierbei Vorteile gegenüber der gewählten globalen Funktion. © 2001 Éditions scientifiques et médicales Elsevier SAS

Statische Aeroelastik / Strömung-Struktur-Kopplung / Mehrfeld Problem / Multivariate Interpolationen / Radiale Basis Funktionen

[1] Correspondence and reprints. Present address: EADS-Military Aircraft Business Unit, PO Box 80 11 60, 81663 München, Germany. Email address: Armin.Beckert@m.dasa.de

1. Introduction

A main task concerning the treatment of coupled aeroelastic systems is the simulation of fluid-structure-interaction (FSI). Research on FSI in the field of numerical aeroelastic simulation has strongly increased in the recent past [6,7,11,12]. An FSI method describes an adequate numerical distribution of aerodynamic loads at the structural nodes of the FE-model – using the aerodynamic pressures given in finite volumes, volume elements, or panels of the discretized flowfield or surface – as well as an adequate deformation of the aerodynamic shape – using the displacements and rotations given at the nodes of the FE-model.

The aeroelastic problem can be described in a coupled field formulation [9,18]. The interaction between the fluid and structural models is limited to the exchange of boundary conditions. Since the fluid and the structural domains show different mathematical and numerical properties, distinct numerical solvers have been developed in the past and a selection of commercial analysis software is available. For the solution of the coupled field problem, these existing well-established numerical solvers can be used. In order to exchange surface loads and surface deformation information (boundary conditions) between the fluid and structural codes, partitioned or staggered procedures for coupling in time [9] and specific schemes for coupling in space can be applied.

In this paper, the main topic is a conservative method for coupling the degrees of freedom of structural nodes and aerodynamic surface points in space. In the recent past both, physically motivated [2,5,19] and mathematically motivated approaches [14,17,29,23] were presented. In this contribution we concentrate on mathematically motivated interpolation schemes using radial basis functions to build the coupling matrix, which can be used for both the transfer of motion and of aerodynamic loads. In the literature, mainly functions without compact support appear to model fluid-structure-interaction. Here, we will compare a typical global method with local methods based on compactly supported radial basis functions. Furthermore, most of the interpolation schemes allow only a coupling in two-dimensional space and are not applicable to more sophisticated non-planar models. Our approach eliminates this problem and can be used in two- and three-dimensional space (actually, in any d-variate space).

The conservative spatial coupling method presented here can be applied to both, static and dynamic cases. We have applied the method only to a typical static aeroelastic problem because in this case time does not appear as a solution variable and only a spatial coupling problem exists. In the dynamic case however, a time-related coupling problem appears additionally and different time integration schemes (for partitioned integration) have to be coupled. Considering only the static case allows us to exclude errors based on time-coupling and to analyze the spatial problem separately.

In the following, the coupled field problem is formulated and a solution procedure is explained. As a main goal a scheme for coupling in three-dimensional space using multivariate interpolation is presented and a selection of radial basis functions is given. Finally, the application due to a static aeroelastic problem is shown.

2. Coupled field problem

The prediction of the static aeroelastic equilibrium of an elastic wing in transonic fluid flow appears in the literature [3,10] as a typical task in Numerical Aeroelasticity. The related fluid-structure-interaction problem can be described in a three-field formulation for the fluid, the structure and the deforming mesh. The set of coupled equations can be written as follows

$$\big(\boldsymbol{A}(\boldsymbol{x})\boldsymbol{w}(\boldsymbol{x})\big)_t + \big(\boldsymbol{F}_1\big(\boldsymbol{w}(\boldsymbol{x})\big)\big)_x + \big(\boldsymbol{F}_2\big(\boldsymbol{w}(\boldsymbol{x})\big)\big)_y + \big(\boldsymbol{F}_3\big(\boldsymbol{w}(\boldsymbol{x})\big)\big)_z = 0, \tag{1}$$

$$\mathcal{G}(\boldsymbol{u}) = \boldsymbol{K}\cdot\boldsymbol{u} = \boldsymbol{f}^{\text{ext}}(\boldsymbol{w},\boldsymbol{x}), \tag{2}$$

$$\boldsymbol{x} = \mathcal{F}(\boldsymbol{u}). \tag{3}$$

Equation (1) represents the transonic inviscid fluid flow that is described by three-dimensional Euler equations.

Here, $\boldsymbol{w}$ is the solution vector, the matrix, $\boldsymbol{A} = \boldsymbol{A}(\boldsymbol{x}, t)$ results from the finite volume discretization and $\boldsymbol{F}_1$, $\boldsymbol{F}_2$, and $\boldsymbol{F}_3$ are the flux vectors with the six primitive variables: density ρ, cartesian components of the velocity u, v, w, pressure p, and specific internal energy e [2,9]. The basic equations of the fluid motion can be derived from the conservation laws of mass, momentum and total energy, neglecting viscosity and heat transfer. The equations are completed by the calorical and thermal equations of state for a perfect gas. The Euler equations are solved by an upwind scheme procedure, using the DLR-τ-Code [22] for the CFD analysis. The variable $\boldsymbol{x}$ is the displacement or position vector of the deforming fluid mesh. Since we are interested in steady state solutions, time t does not appear explicitly as a solution variable. The fluid state equations are solved for each iterative solution step and for the related position vector $\boldsymbol{x}$, as shown later.

The Euler equations do not take viscosity into account, but they are able to describe nonlinear effects in the solution as they appear in transonic fluid flow. In industry, for aeroelastic computations still linear aerodynamic models are applied. For some cases and for certain flow conditions, more precise aerodynamic models are used to correct the linear results. Widely used are the Euler equations, with or without Boundary-Layer-Coupling, because the solution of the Navier–Stokes equations is very (time) expensive and the Euler equations seem to be

more robust for the application in Numerical Aeroelasticity and the prediction of a completely unknown fluid flow.

In this contribution, the material areas and the relevant elastic behaviour of the structure are discretized by finite elements [1]. Equation (2) is the classical linear formulation of the elastostatic equilibrium state where $\boldsymbol{u}$ denotes the vector of the displacements at the structural nodes. $\boldsymbol{K}$ is the global linear stiffness matrix of the finite element model, and $\boldsymbol{f}^{\text{ext}}$ denotes the load vector of external (aerodynamic) forces acting at the finite element nodes. In the following, it is assumed that the displacement vector $\boldsymbol{u}$ in equation (2) is a linear function of the force vector $\boldsymbol{f}^{\text{ext}}$ within each iterative solution step of the static aeroelastic equations. The stiffness matrix $\boldsymbol{K}$ and load vector $\boldsymbol{f}^{\text{ext}}$ are determined by integrating over the volume of the undeformed finite elements and the material is assumed to be linearly elastic. The finite element equations are solved using the commercial FE analysis program Permas [28].

Finally, equation (3) governs the deformation of the finite volume mesh of the fluid. Here, the dynamic or deforming mesh is represented by a pseudo-structural system [8]. The related grid deformation method prolongates the surface deformation into the field by a front method [13]. In (3), the position vector $\boldsymbol{x}$ of the fluid mesh nodes is a function of the vector $\boldsymbol{u}$ of the structural displacements given at the finite element nodes. The equations (1) and (3) are coupled within the position vector $\boldsymbol{x}$ of the fluid mesh nodes, whereas (2) and (3) are coupled by the structural displacement vector $\boldsymbol{u}$.

The coupled nonlinear aeroelastic equations are solved by a fixed-point iteration scheme belonging to a set of conventional serial staggered procedures (CSS) [2, 9], that allow the determination of the structural and fluid solution vector independently from each other, updating afterwards the relevant boundary conditions (*figure 1*). In order to solve the basic equations, different numerical solution schemes and commercial analysis software are applied. The CSS iterative solution scheme, in the case of static aeroelastic stability, leads to the static aeroelastic equilibrium which requires that the (external) aerodynamic loads and their elastomechanical reaction forces of the structure are in a state of equilibrium. A further description of the solution scheme can be found in the literature [2,9].

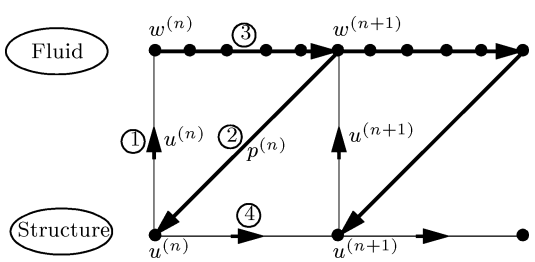

Figure 1. Conventional serial staggered procedure.

3. Fluid-structure interaction

Because both the aerodynamic and structural models are discretized in a physically different manner, they do not match at the boundary. This means that generally the models do not share the same nodes at their common boundary. Consequently, the structural discretization is not constrained to model the aerodynamic shape in such a manner that there have to be elements or nodes to represent a sufficiently smooth surface. While the spatial discretization of the flow field is based on a finite volume formulation using Eulerian coordinates, the structural model consists of finite elements in a Lagrangian description.

The coupled approach allows independent discretization and refinement of the areas of physical interest and keeps the independence of the structural and fluid domain. The boundary conditions of the related coupling scheme are given by the discrete aerodynamic surface of the elastic body in the flow field with the relevant pressures and the finite element structure with its corresponding displacements and rotations at its element nodes. It must transform the aerodynamic loads into respective work equivalent forces at the finite element nodes and calculate displacements at the aerodynamic surface mesh using displacements and rotations of the structural model.

3.1. Equivalence of work

The coupling scheme has to preserve the equivalence of virtual work performed by the (external) aerodynamic loads and the (internal) structural forces (stresses)

$$\delta W = \delta \boldsymbol{u}_s^{\mathsf{T}} \cdot \boldsymbol{f}_s = \delta \boldsymbol{u}_f^{\mathsf{T}} \cdot \boldsymbol{f}_f. \tag{4}$$

The fluid-structure-interaction can be expressed in a linear approximation by introducing a coupling matrix $\boldsymbol{H}$, that relates the displacement vectors in x-, y- and z-direction of the finite element structure and the fluid mesh [17]

$$\boldsymbol{u}_f = \boldsymbol{H} \cdot \boldsymbol{u}_s. \tag{5}$$

When it is assumed that the virtual work δW is equal to zero for arbitrary δu_s, the relation between the virtual displacements of the structure and the aerodynamic mesh can be achieved

$$\delta \boldsymbol{u}_f = \boldsymbol{H} \cdot \delta \boldsymbol{u}_s.$$

From equations (4) and (5) it follows

$$\boldsymbol{f}_s = \boldsymbol{H}^{\mathsf{T}} \cdot \boldsymbol{f}_f, \tag{6}$$

with $\boldsymbol{H}^{\mathsf{T}}$ as the transposed of the coupling matrix $\boldsymbol{H}$. When a coupling matrix $\boldsymbol{H}$ exists that satisfies the equations as mentioned above, it can be used for both,

the transformation of the displacements of the structure and as its transposed, for the transformation of the aerodynamic loads [2,17].

3.2. Coupling scheme using multivariate interpolation

In the following, a coupling scheme is presented which uses multivariate interpolation for load and motion transfer in three-dimensional space. The relation between the fluid and the structural model is expressed within a coupling matrix as shown in the previous subsection.

For the use of multivariate interpolation, first, the pressure values are integrated over the surface area of the aerodynamic cells and transformed into orthogonally acting forces with respect to the cell surface. A conservative coupling scheme requires the integration of the aerodynamic pressure on the aerodynamic surface (boundary) where it acts, instead of computing respective pressure values on the finite elements of the structural model.

The scheme presumes the definition of sets of evaluation nodes and of nodes with given values, the so-called centers. For the interpolation of displacement information the centers are represented by the structural nodes, whereas for the load transformation by the aerodynamic surface mesh nodes. The sets include the nodes of the CFD surface mesh, where the (aerodynamic) external forces act and the finite element nodes, on which those forces are transformed [3]. The selection of finite element nodes may enclose all at the free surfaces of the structural model or only a portion. It is of importance that only those structural nodes are considered, which are able to support the degrees of freedom provided by the coupling scheme. Topology information of the aerodynamic surface mesh and the structural model is not necessary, since the interpolation scheme is applicable to both scattered and gridded data [4].

In order to compute a displacement field $\boldsymbol{u}$

$$\boldsymbol{u} = \boldsymbol{C}_{ss} \cdot \boldsymbol{p}, \tag{7}$$

the coefficients $\boldsymbol{p}$ for a given solution $\boldsymbol{u}_s$ have to be computed first,

$$\boldsymbol{p} = \boldsymbol{C}_{ss}^{-1} \cdot \boldsymbol{u}_s. \tag{8}$$

In (7) and (8), $\boldsymbol{C}_{ss}$ is the interpolation matrix coming from the radial basis function approach, as is explained in the next subsection. The entries depend on the chosen basis function and the given displacements $\boldsymbol{u}_s$ at the structural nodes $\boldsymbol{s}_j$.

Assuming that a deformation state can be described as a linear combination of unit displacements, it follows

$$\boldsymbol{U}_s = \boldsymbol{C}_{ss} \cdot \boldsymbol{P} \tag{9}$$

with the matrix $\boldsymbol{U}_s$ representing the unit displacements along all degrees of freedom of the system

$$\boldsymbol{U}_s = \begin{pmatrix} 1 & 0 & \dots & 0 \\ 0 & 1 & \dots & 0 \\ \vdots & \vdots & \ddots & 0 \\ 0 & 0 & \dots & 1 \end{pmatrix}.$$

The aerodynamic displacements that correspond to any linear combination of the structural displacements $\mathbf{U}_s$ can be determined by

$$\boldsymbol{U}_f = \boldsymbol{A}_{fs} \cdot \boldsymbol{P} = \boldsymbol{A}_{fs} \cdot \boldsymbol{C}_{ss}^{-1} \cdot \boldsymbol{U}_s, \tag{10}$$

where $\boldsymbol{A}_{fs}$ is the matrix corresponding to the evaluation of the interpolant at the aerodynamic nodes and $\boldsymbol{P}$ is the matrix of coefficients as shown in equation (9). Equation (10) contains the definition of the coupling matrix $\boldsymbol{H}$ which relates the aerodynamic displacements to the structural ones as mentioned in equation (5)

$$\boldsymbol{H} = \boldsymbol{A}_{fs} \cdot \boldsymbol{C}_{ss}^{-1}. \tag{11}$$

In the following subsections the construction of the coupling matrix $\boldsymbol{H}$ and the matrices $\boldsymbol{A}_{fs}$ and $\boldsymbol{C}_{ss}^{-1}$ is shown.

3.3. Radial basis functions

Radial basis functions have become a well-established tool for multivariate interpolation of both scattered and gridded data [4,17,21,25]. Some classical radial basis functions which provide good approximation behaviour and that are widely used for two-dimensional problems in engineering, are Duchon's thin plate splines

$$\phi(\|\boldsymbol{x}\|) = \|\boldsymbol{x}\|^2 \log(\|\boldsymbol{x}\|),$$

Hardy's multiquadrics

$$\phi(\|\boldsymbol{x}\|) = \left(c^2 + \|\boldsymbol{x}\|^2\right)^{1/2},$$

and inverse multiquadrics

$$\phi(\|\boldsymbol{x}\|) = \left(c^2 + \|\boldsymbol{x}\|^2\right)^{-1/2}$$

[16]. Recently, the functions have been applied in many fields of CAD and CAE. Here as a specific issue, radial basis functions are used for fluid-structure-interaction problems in the field of Numerical Aeroelasticity.

We will continue to describe the general concept of radial basis function interpolation now in more detail and apply it to a fluid-structure-interaction problem in the next subsection to derive the coupling matrix $\boldsymbol{H}$.

A general multivariate interpolation problem can be described as follows: Suppose a set of pairwise distinct points $X = \{\boldsymbol{x}_1, \ldots, \boldsymbol{x}_N\} \subseteq \mathbb{R}^d$ in the d-variate Euclidean space is given. These points are normally called 'centers'. Suppose further, we know values $g_1, \ldots, g_N$ at the centers and we are searching for a continuous function that interpolates these values at the centers. Then the radial basis function interpolant has the form

$$s_{g,X}(\boldsymbol{x}) = \sum_{j=1}^{N} \alpha_j \phi(\|\boldsymbol{x} - \boldsymbol{x}_j\|) + p(x). \tag{12}$$

In (12) the function $\Phi := \phi(\|\cdot\|)$ is a fixed basis function which is radial with respect to the Euclidean distance

$$\|\boldsymbol{x}\| = \sqrt{x_1^2 + \cdots + x_d^2},$$

and p is a low degree d-variate polynomial. The coefficients α_j and the polynomial p are determined by the interpolation conditions

$$s_{g,X}(\boldsymbol{x}_j) = g_j, \quad 1 \leqslant j \leqslant N, \tag{13}$$

and the additional requirements

$$\sum_{j=1}^{N} \alpha_j q(x_j) = 0 \tag{14}$$

for all polynomials q with a degree $\deg(q) \leqslant \deg(p)$. The minimal degree of the polynomial depends on the choice of the basis function ϕ. A unique interpolant is given if the basis function Φ is a conditionally positive definite function.

DEFINITION 3.1. – *An even function $\Phi : \mathbb{R}^d \to \mathbb{R}$ is said to be conditionally positive definite of order m if for all $N \in \mathbb{N}$, all sets of pairwise distinct centers $X = \{\boldsymbol{x}_1, \ldots, \boldsymbol{x}_N\} \subseteq \mathbb{R}^d$ and all $\alpha \in \mathbb{R}^N \setminus \{0\}$ that satisfy* (14) *for all polynomials q of degree less than m, the quadratic form*

$$\sum_{j=1}^{N} \sum_{k=1}^{N} \alpha_j \alpha_k \Phi(\boldsymbol{x}_j - \boldsymbol{x}_k)$$

is positive.

As said before, the benefit of this definition is that it guarantees a unique interpolant. However, before we state this result let us remark that every conditionally positive definite function of order m is obviously also conditionally positive definite of order $\tilde{m} \geqslant m$. Thus an increase of the polynomial degree of the polynomial in (12) is always possible and sometimes reasonable. Furthermore, note that in case of a conditionally positive definite function of order $m = 0$ the conditions (14) are empty and thus the quadratic form in the definition has to be positive for all $\alpha \not\equiv 0$. Such functions are normally called 'positive definite'.

THEOREM 3.1. – *Suppose Φ is conditionally positive definite of order m. Suppose further that the set of centers $X = \{\boldsymbol{x}_1, \ldots, \boldsymbol{x}_N\}$ has the property that the zero polynomial is the only polynomial of degree less than m that vanishes on it completely. Then there exists exactly one function $s_{g,X}$ of the form* (12) *that satisfies both* (13) *and* (14).

The simple proof of this theorem can be found in [20, 25]. The additional requirements on X form only a mild condition. For example, if we work with linear polynomials on $\mathbb{R}^3$, X has only to contain 4 points that do not lie on a plane.

Condition (14) together with this uniqueness result has an important consequence. Suppose we work with conditionally positive definite functions of order $m = 2$. Then the polynomial in the interpolant is a linear polynomial. If the data values g_j come from a linear polynomial g themselves, i.e. $g_j = g(\boldsymbol{x}_j)$ this polynomial is exactly reproduced.

3.4. Coupling matrix based on radial basis function interpolation

Coming back to the fluid-structure-interaction, we assume that we have N_s structural nodes $\boldsymbol{s}_j = (x_{s_j}, y_{s_j}, z_{s_j})^{\mathrm{T}} \in \mathbb{R}^3$, $1 \leqslant j \leqslant N_s$, and N_f aerodynamic nodes $\boldsymbol{f}_j = (x_{f_j}, y_{f_j}, z_{f_j})^{\mathrm{T}} \in \mathbb{R}^3$, $1 \leqslant j \leqslant N_f$, and we want to recover the aerodynamic displacements from the structural displacements $u(\boldsymbol{s}_j)$. Thus the centers are the structural nodes and the structural displacements are the values we want to interpolate. Actually, we have three interpolation problems, one for every direction.

Here, we will only use basis functions that are conditionally positive definite of order $m \leqslant 2$. This means we can always form the interpolant using linear polynomials, i.e. p will have the form

$$p(\boldsymbol{x}) = \alpha_0 + \alpha_1 \cdot x + \alpha_2 \cdot y + \alpha_3 \cdot z. \tag{15}$$

Remember that a conditionally positive definite function of order $m = 0, 1$ is also conditionally positive definite of order $m = 2$ which justifies our proceeding. This has the additional advantage that linear polynomials are exactly reproduced which means in this context that rigid body translations are exactly recovered.

The coupling matrix $\boldsymbol{H}$ can be determined by multiplying $\boldsymbol{A}_{fs}$ and $\boldsymbol{C}_{ss}^{-1}$, as equation (11) shows. The symmetric matrix $\boldsymbol{C}_{ss}$ can now be written as follows

$$\boldsymbol{C}_{ss} = \begin{pmatrix} 0 & 0 & 0 & 0 & 1 & 1 & \cdots & 1 \\ 0 & 0 & 0 & 0 & x_{s_1} & x_{s_2} & \cdots & x_{s_{N_s}} \\ 0 & 0 & 0 & 0 & y_{s_1} & y_{s_2} & \cdots & y_{s_{N_s}} \\ 0 & 0 & 0 & 0 & z_{s_1} & z_{s_2} & \cdots & z_{s_{N_s}} \\ 1 & x_{s_1} & y_{s_1} & z_{s_1} & \phi_{s_1 s_1} & \phi_{s_1 s_2} & \cdots & \phi_{s_1 s_{N_s}} \\ 1 & x_{s_2} & y_{s_2} & z_{s_2} & \phi_{s_2 s_1} & \phi_{s_2 s_2} & \cdots & \phi_{s_2 s_{N_s}} \\ \vdots & \vdots & \vdots & \vdots & \vdots & \vdots & \ddots & \vdots \\ 1 & x_{s_{N_s}} & y_{s_{N_s}} & z_{s_{N_s}} & \phi_{s_{N_s} s_1} & \phi_{s_{N_s} s_2} & \cdots & \phi_{s_{N_s} s_{N_s}} \end{pmatrix}. \tag{16}$$

In order to get the values $\phi_{s_i s_j} = \phi(\|\boldsymbol{s}_i - \boldsymbol{s}_j\|)$, the radial basis function has to be evaluated only on structural nodes, whereas in the matrix $\boldsymbol{A}_{fs}$

$$\boldsymbol{A}_{fs} = \begin{pmatrix} 1 & x_{f_1} & y_{f_1} & z_{f_1} & \phi_{f_1 s_1} & \phi_{f_1 s_2} & \cdots & \phi_{f_1 s_{N_s}} \\ 1 & x_{f_2} & y_{f_2} & z_{f_2} & \phi_{f_2 s_1} & \phi_{f_2 s_2} & \cdots & \phi_{f_2 s_{N_s}} \\ \vdots & \vdots & \vdots & \vdots & \vdots & \vdots & \ddots & \vdots \\ 1 & x_{f_{N_f}} & y_{f_{N_f}} & z_{f_{N_f}} & \phi_{f_{N_f} s_1} & \phi_{f_{N_f} s_2} & \cdots & \phi_{f_{N_f} s_{N_s}} \end{pmatrix} \tag{17}$$

they depend on both aerodynamic and structural nodes. In the following a selection of radial basis functions is reviewed which are applicable to three-dimensional fluid-structure-interaction problems.

3.4.1. Volume Spline function

The Volume Spline function can be seen as an extension of the Surface Spline function [14,29] and was first presented by Hounjet and Meijer [17] in this context. Its interpolant has been described in equation (12), using a linear polynomial as shown in equation (15). The radial basis function,

$$\phi(\|\boldsymbol{x}\|) = \|\boldsymbol{x}\| \tag{18}$$

is the Euclidean distance itself, which is conditionally positive definite of order $m = 1$ (actually, $-\phi$ is conditionally positive definite of order $m = 1$). Since ϕ is an increasing function the influence of a center on an evaluation node is the bigger the more distant those two nodes are one from each other. This global character of the function tends to smooth out local effects that may occur in the solution of coupled aeroelastic equations. Furthermore, the interpolation matrix $\boldsymbol{C}_{ss}$ is dense and the evaluation of the interpolant (12) needs an evaluation of all N summations. From a practical and physical point of view, this is not a desirable feature for the application in fluid-structure-interaction.

In order to eliminate the disadvantages of global basis functions as the Volume Splines, those with a so-called 'compact support' can be used. Smooth compactly supported radial functions have recently been constructed and presented [21,25,26]. In the following subsections, a selection of such functions are shown. All of these function are positive definite (i.e. conditionally positive definite of order $m = 0$).

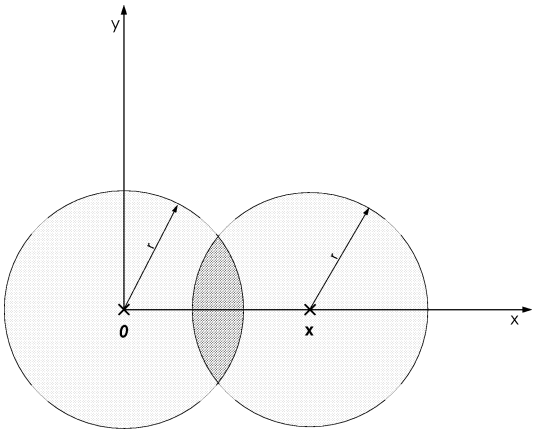

Figure 2. Intersection of spheres.

3.4.2. Euclids Hat function

The Euclids Hat function was first presented by Wendland ([24], see also [21]). It can be used for three-dimensional multivariate interpolation as described in equation (12) but shows contrary to the Volume Spline function, a continuous compactly supported radial basis function

$$\phi(\|\boldsymbol{x}\|) = \pi \cdot \left(\left(\frac{1}{12} \cdot \|\boldsymbol{x}\|^3 \right) - \left(r^2 \cdot \|\boldsymbol{x}\| \right) + \left(\frac{4}{3} \cdot r^3 \right) \right) \tag{19}$$

that has at $\boldsymbol{x}$ the value of the intersection volume of two spheres with radius r, as shown in *figure 2*. This value becomes maximal for two identical nodes and zero for two nodes that are more distant than $(2 \cdot r)$. With the compact support controlled by the value of the radius r, the function shows a flexible local character. Further information on smoothness and mathematical features can be found in the related literature [24].

3.4.3. Compactly supported functions introduced by Wendland

Recently, Wendland [25,26] constructed further examples of smooth compactly supported radial basis functions. He proved that these, for a specific space dimension d, possess the lowest possible degree among all piecewise polynomial compactly supported radial functions which are positive definite on $\mathbb{R}^d$ and of a given order of smoothness, which is a useful property in practice. In this context we will use only the C^0- and the C^2-function for space dimension $d = 3$:

$$\phi(\|\boldsymbol{x}\|) = (1 - \|\boldsymbol{x}\|)_+^2, \quad C^0, \tag{20}$$

$$\phi(\|\boldsymbol{x}\|) = (1 - \|\boldsymbol{x}\|)_+^4 \cdot (4 \cdot \|\boldsymbol{x}\| + 1), \quad C^2. \tag{21}$$

Especially the C^2-function, which is shown in *figure 3*, leads to promising results.

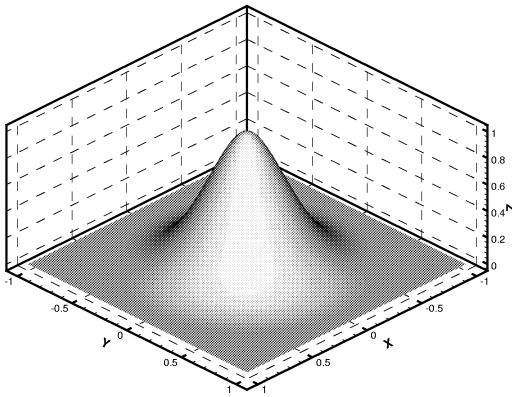

Figure 3. Wendland's C^2-function.

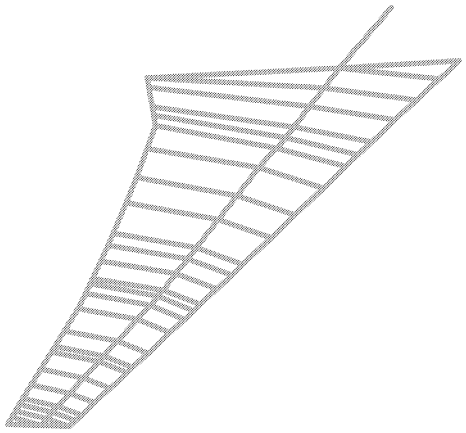

Figure 4. Structural finite element model.

3.4.4. Choice of support radius

The compactly supported radial basis functions of the last two subsections lead to the question of how to choose the support radius of these functions. First of all, since scaling does not influence the property of a function to be positive definite, we define the function $\phi_\rho(t) = \phi(t/\rho)$ with ϕ given by any of the previously mentioned functions. This means that ϕ_ρ is a positive definite function with support radius $r = 2\rho$ in case of Euclid's Hat and radius $r = \rho$ in case of Wendland's functions. The parameter ρ allows us to adapt the support radius to our problem making sure that on the one hand there are enough points covered and on the other hand points being far away have no influence. It would be very useful if we could vary the radius from center to center, but the theory only guarantees solvability for a 'fixed' radius, even if numerical experiments show that in most cases a variable support leads to a solution.

However, even in the situation of a fixed radius the choice of it is delicate. From the mathematical point of view a large support radius (compared to the data density) yields a good approximation order while a small support radius leads to a stable system that can easily be solved. This trade off principle is also reflected in our application.

In practice, a reasonable fixed support radius for the fluid-structure-interaction problem has to guarantee a full coverage of the interpolation space. The region that is influenced by a center, is represented by a sphere with radius r that should include at least all nearest neighbors of the considered center. Since the aeroelastic model consists of both, a structural model and an aerodynamic surface mesh, also its nearest neighbors in the respective other discretization have to be found. For some applications this condition is not sufficient, so that the sphere should also cover the points of the finite or surface element in which the center is a member. The fixed support radius for the presented fluid-structure-interaction problem is chosen to be the largest support radius of all centers.

4. Applications

In the following, we consider the static aeroelastic analysis of a wind tunnel model. All static aeroelastic computations were performed using the same partitioned solution procedure to solve the coupled field problem. For the coupling in space, the above presented multivariate interpolation scheme is used by varying the radial basis function.

During the Aeroelastic Model Program (AMP) a transport aircraft wing was examined in wind tunnel testing for static and dynamic aeroelastic purposes [15,27]. Here, the experimental data of the AMP program are used to verify the numerical results of the static aeroelastic computations. These are pressures and displacements of the wing structure measured during wind tunnel tests for several test cases. For the computations however, a Mach number of $M_\infty = 0.82$, and an angle of attack $\alpha = 2.55°$ were chosen [3]. The AMP model was chosen for this paper because it is still of interest for the European aerospace industry and the former partners of the AMP. Further information about the aeroelastic model, and also the experimental and numerical results are documented in [3, 15,27]. Since the availability of the detailed numerical model data is restricted, we suggest to those who are interested in this information to contact the authors of [15, 27] directly.

The structural model (*figure 4*) of the wind tunnel configuration was built using finite elements and updated in order to represent the static and dynamic behaviour of the real structure [2,3]. It consists of 25 finite beam elements that are situated along the line of elastic centers of the structure. The ribs of the wing are represented by rigid lever arms orthogonal to the elastic axis. The structure is connected to a system of torsional and longitudinal spring elements that represent an elastic support. The structural finite element equations are solved by the commercial finite element analysis program Permas [28]. The aerodynamic model of the AMP wing describes the

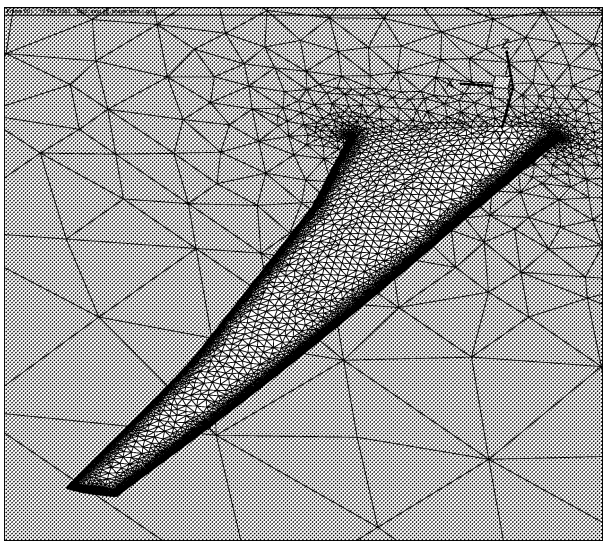

Figure 5. Spatial discretization of the flow field.

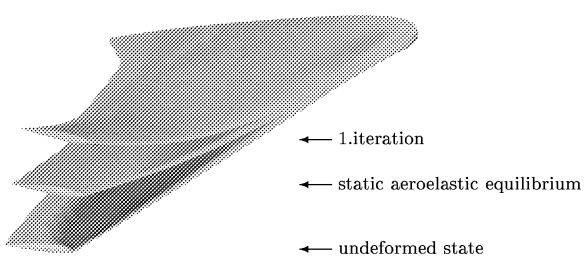

Figure 6. Deformation states during iterative solution.

three-dimensional, compressible fluid flow by the nonlinear Euler equations, solved by a specific upwind-scheme using the DLR-τ-Code [22] for the CFD analysis. For the spatial discretization, an unstructured finite volume mesh was generated which contains 1437101 tetraeders and 271482 vertices. The wing surface is discretized by 109216 surface triangles and 54653 vertices (*figure 5*).

The deforming AMP wing shows a chordwise camber bending in flow direction. This is a well-known phenomenon of backward swept wings, because only along the line of shear centers of the various cross sections (elastic axis), the torsion and bending motion of the structure are decoupled. Since the measurement points are situated along lines in the flow direction where camber bending appears, it would be incorrect to assign chordwise torsion angles. In the wind tunnel tests torsion angles have not been measured but only computed as a linear approximation using the difference between the displacements of two neighboring nodes given in flow direction. In reference [27], the measured displacements and the computed torsional angles are presented. However, since in the wind tunnel tests torsion angles have not been measured only

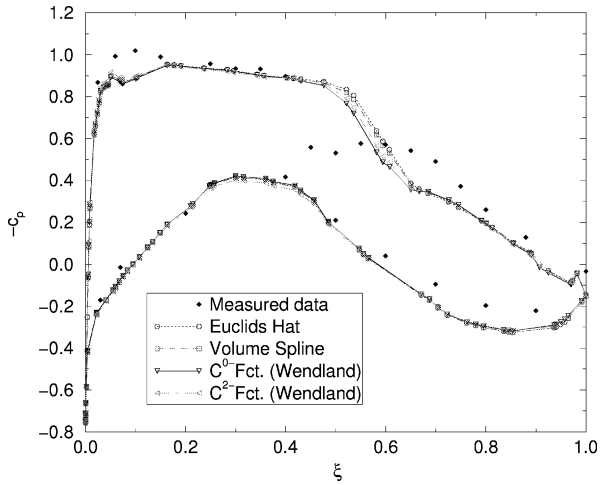

Figure 7. Pressure distribution at 37% span.

the measured displacements are used here for the comparison with the numerical results.

For the chosen test case ($M_\infty = 0.82$, $\alpha = 2.55°$) convergence was reached after 8 iterative steps for all radial basis functions. In *figure 6* the undeformed state, the deformation state after the first iterative solution step and the equilibrium state of the aerodynamic surface are shown for the application of the Euclids Hat function. The region of the surface showing high lift values is seen to decrease during the deformation.

Figure 7 shows the pressure distribution ($-c_p$) at 37% span in the aeroelastic equilibrium state for the selection of radial basis functions in comparison to the measured data. The curves of the computed pressure distribution show differences especially on the upper surface in the region of high velocities and low pressure near the leading edge and also in the region of the shock. Its position is not reproduced well, due to the used aerodynamic model. This phenomenon is a well-known deficiency of the Euler equations which arises because viscous effects are ignored. The consequences are incorrect lift and moment values, especially for higher Mach numbers, when nonlinear effects become important in the solution. For the $M_\infty = 0.82$ test case the difference between measured lift values and the related numerical results are for the Volume Spline function 7.8%, for the Euclids Hat function 8%, for the C^0-function presented by Wendland 5.2% and the C^2-function 8%, with respect to the measured values.

In *figure 8* the related z-displacements along the elastic axis of the structural model are shown. The maximum differences between measured and computed displacements with respect to the measured values at the wing tip are 5.6% for the Volume Spline, 6% for the Euclids Hat, 10% for the C^2-function presented by Wendland and 20% for the C^0-function. At this point, especially the Euclids Hat, the Volume Spline and the C^2-function introduced by Wendland can be seen to show

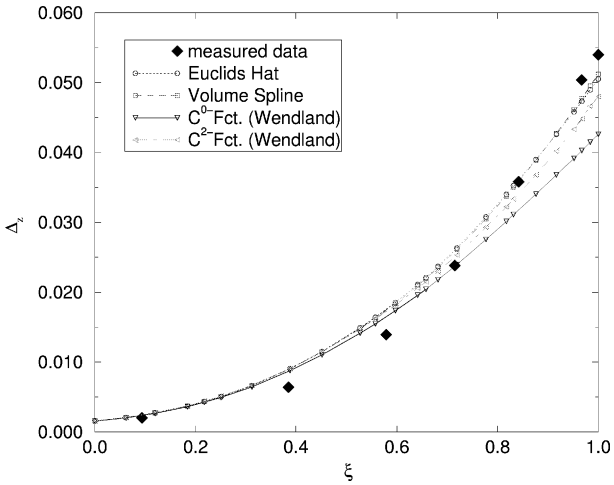

Figure 8. Semispan displacements due to aeroelastic computations.

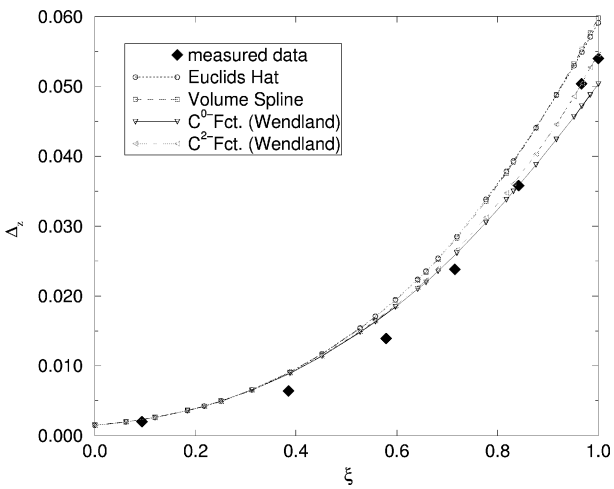

Figure 9. Semispan displacements due to measured pressure distribution.

satisfactory results. Nevertheless, for an interpretation of the shown solutions, the influence of the coupling scheme and the aerodynamic model have to be considered.

Obviously, the CFD model and its discretization influence the solution of the coupled aeroelastic problem remarkably [3]. In order to find out which influence the aerodynamic model (Euler equations) has on the computed aeroelastic equilibrium, the measured pressure distribution was applied to the structural finite element model, as if determined within a numerical computation, using the coupling schemes. *Figure 9* shows the resulting displacements in spanwise direction. The curve of the C^2-function, is seen to be close to the measured displacement values. At the tip of the wing the difference between the computed and the measured displacements is 0.05% for the C^2 Wendland function, whereas for the Volume Spline the difference is 9.8%, for the Euclids Hat 8.9% and for the C^0-function 6.4%, with respect to the measured values.

As a result it follows that the differences between the computed and measured values are attributed to both the aerodynamic model used, that does not describe the fluid flow correctly and in part to the coupling scheme, that is responsible for an adequate numerical distribution of the computed aerodynamic loads on the structural model. Concerning the chosen numerical aerodynamic model, it has to be mentioned that the Euler equations, in contrast to the Navier–Stokes equations, describe an inviscid flow. The neglection of viscosity, especially when considering a transsonic flow, conributes to the disagreement of numerical and experimental results. Comparing the curves of the selection of functions with the measured values and using the measured pressure as a reference, in particular the (C^2)-function shows satisfactory conformity.

5. Conclusions

This contribution presents a conservative coupling scheme for numerical aerodynamic (CFD) and structural (FE) models, that transforms aerodynamic and elastomechanical data on non-planar configurations and is based on multivariate interpolation using smooth compactly supported radial basis functions. The coupling algorithm maintains its independence from the CFD and FE models and the corresponding solution schemes so that these methods allow the interchange of different aerodynamic and elastomechanical analysis tools and models. Furthermore, local nonlinear effects appearing in aerodynamic and structural models may be taken into account.

The application of the coupling scheme to a typical static aeroelastic problem is shown. The comparison of the numerical results, achieved by the computation of the static aeroelastic equilibrium of a wind tunnel configuration and the related experimental data measured during wind tunnel tests, shows satisfactory conformity. The differences between the computed and measured values are attributed to both the coupling scheme, that is responsible for an adequate numerical distribution of the computed aerodynamic loads on the structural model, and the choosen numerical aerodynamic model (Euler equations), that does not describe the fluid flow correctly neglecting its viscosity.

For the chosen test case and using the measured pressure as a reference, the multivariate interpolation scheme using radial basis functions with compact support are seen to be more advantageous compared to the global function.

References

[1] Bathe K.-J., Finite Elemente-Methoden, Springer-Verlag, Heidelberg-Berlin-New York, 1986.

[2] Beckert A., Coupling fluid (CFD) and structural (FE) models using finite interpolation elements, Aerosp. Sci. Technol. 4 (1) (2000) 13–22.

[3] Beckert A., Ein Beitrag zur Strömungs-Struktur-Kopplung zur Berechnung des aeroelastischen Gleichgewichts, Ph.D. Thesis, ISRN DLR-FB–97-42, Göttingen, 1997.

[4] Buhmann M.D., New developments in the theory of radial basis function interpolation, in: Jetter K., Utreras F.I. (Eds.), Multivariate Approximation: from CAGD to Wavelets, World Scientific, Singapore, 1993, pp. 35–75.

[5] Cebral J.R., Löhner R., Conservative load projection and tracking for fluid-structure problems, AIAA J. 35 (4) (1997).

[6] Done G.T., Past and Future Progress in Fixed and Rotary Wing Aeroelasticity, London, City University Press, 1992, pp. 23.1–23.8.

[7] Edwards J.W., Computational aeroelasticity, in: Flight-Vehicles, Materials, Structures and Dynamics – Assessment and Future Directions, Vol. 5, The American Society of Mechanical Engineers, New York, NY 10017, 1993.

[8] Farhat C., Degand C., Koobus B., Lesoinne M., An improved method of spring analogy for dynamic unstructured fluid meshes, AIAA 98-2070, 39th AIAA/ASME/ASCE//AHS Structures, Structural Dynamics and Materials Conference, Long Beach, CA, 1998.

[9] Farhat C., Lesoinne M., Higher-order staggered and subiteration free algorithms for coupled dynamic aeroelasticity problems, 36th Aerospace Sciences Meeting and Exhibit, AIAA 98-0516, Reno/NV, 1998.

[10] Försching H., Grundlagen der Aeroelastik, Springer-Verlag, Heidelberg-Berlin-New York, 1974.

[11] Försching H., New Ultra High Capacity Aircraft (UHCA) – Challenges and problems from an aeroelastic point of view, Z. Flugwiss. Weltraum. 18 (4) (1994) 219–231.

[12] Försching H., Challenges and perspectives in computational aeroelasticity, in: Proc. of the International Forum on Aeroelasticity and Structural Dynamics, Manchester, UK, Vol. 1, 1995, pp. 1.1–1.9.

[13] Gerhold T., Weinmann K., Günther G., Schwamborn D., Beckert A., Application of the DLR-TAU Code to fluid-structure interactions on hybrid grids, Eccomas 2000, Barcelona, Spain, 2000.

[14] Harder R.L., Desmarais R.N., Interpolation using surface splines, J. Aircraft 9 (1972) 189–197.

[15] Hönlinger H., Manser R., Gravelle A., Viguier P., Measurement of wind tunnel model deformation under airload, European Forum on Aeroelasticity and Structural Dynamics, Aachen, DGLR-Bericht 91-069, 1991.

[16] Hoschek J., Lasser D., Grundlagen der geometrischen Datenverarbeitung, B.G. Teubner Verlag, 1992.

[17] Hounjet M.H.L., Meijer J.J., Evaluation of elastomechanical and aerodynamic data transfer methods for non-planar configurations in computational aeroelastic analysis, ICAS-Publication, 1994, pp. 10.1–10.25.

[18] Kutler P., Multidisciplinary computational aerosciences, in: Proc. of the 5th Int. Symp. on Comp. Fluid Dynamics, Sendai, 1993, pp. 109–119.

[19] Maman N., Farhat C., Matching fluid and structure meshes for aeroelastic computations: a parallel approach, Comput. Struct. 54 (1995) 779–785.

[20] Madych W.R., Nelson S.A., Multivariate interpolation and conditionally positive definite functions, Approx. Theory and its Appl. 4 (1988) 77–89.

[21] Schaback R., Creating surfaces from scattered data using radial basis functions in: Dæhlen M., Lyche T., Schumaker L. (Eds.), Mathematical Methods for Curve and Surfaces, Vanderbilt University Press, Nashville, 1995, pp. 477–496.

[22] Schwamborn D., Gerhold T., Kessler R., The DLR-TAU Code – an Overview, ONERA-DLR Aerospace Symposium, Paris, France, 1999.

[23] Smith M.J., Cesnik C.E.S., Hodges D.H., An evaluation of computational algorithms to interface between CFD and CSD methodologies, AIAA Struct., Struct. Dyn., Materials, 37, 1996, pp. 745–755.

[24] Wendland H., Ein Beitrag zur Interpolation mit radialen Basisfunktionen, Diplomarbeit Universität Göttingen, 1994.

[25] Wendland H., Konstruktion und Untersuchung radialer Basisfunktionen mit kompaktem Träger, Dissertation Universität Göttingen, 1996.

[26] Wendland H., Piecewise polynomial, positive definite and compactly supported radial basis functions of minimal degree, Adv. Comput. Math. 4 (1995) 389–396.

[27] Zingel H., Jajes U., Vogel S., Aeroelastisches Modellprogramm I, Stationäre und instationäre Luftkräfte, Deutsche Airbus DA/BRE/91-111, 1991.

[28] Intes, PERMAS – Theory Manual, Stuttgart, INTES Publication No. 302, 1987.

[29] MacNeal-Schwendler Corp., NASTRAN – Handbook for Aeroelastic Analysis I/II, 1987.